International Journal of Signal Processing, Image Processing and Pattern Recognition
Vol.8, No.11 (2015), pp.75-84
http://dx.doi.org/10.14257/ijsip.2015.8.11.08

Multi-modal Medical Image Fusion Based on the Multiwavelet and Nonsubsampled Direction Filter Bank

Peng Geng[*1], Xing Su[1], Tan Xu[2] and Jianshu Liu[3]

[1]*School of Information Science and Technology, Shijiazhuang Tiedao University, Shijiazhuang, China 050043*
[2]*Department of Physics and Electronic Information, Hengshui University, Hengshui, China 053000*
[3]*Shijiazhuang Appraisal Center of Vocation Skill and Teaching Research, Shijiazhuang, China 050000*
GengPeng@stdu.edu.cn

Abstract

Aiming at solving the fusion problem of multimodal medical images, a novel medical image fusion algorithm is present in this paper. The multiwavelet is combined with the NSDFB to construct the proposed Multi-NSDFB transform. The source images can be decomposed into several lowpass coefficient and highpass coefficient. And all coefficients can be decomposed into four direction subbands. The modified spatial frequency is adopted to motivate the pulse coupled neural network to select the every direction subbands coefficients. Experiment results demonstrate that the proposed algorithm can not only extract more important visual information from source images, but also effectively avoid the introduction of artificial information. The present scheme outperforms the redundant discrete wavelet transform-based, and the Ripplet transform-based in terms of both visual quality and objective evaluation.

Keywords: *image fusion, nonsubsampled direction filter bank, multi-modal medical image*

1. Introduction

With the development of medical technology, computer science and biomedical engineering technology, the medical image technology can provide the clinical diagnosis with a variety of multi-modal medical images such as the computed tomography (CT), the magnetic resonance imaging (MRI), the single photon emission computed tomography (SPECT), the positron emission tomography (PET) and ultrasonic images [1]. Different medical image can display different information of the same viscera in the body. For example, The MRI is good at express the soft tissue information than the CT is. However, the CT image can provide better information of tissue calcification and bone segment than the MRI can. In the clinic application, a single modal of medical image often cannot provide enough information to doctors to make the right diagnosis. It is necessary to combine different modal images to one image with enough information of source images. The fused medical images can contain the vital information from the several modal images to demonstrate the comprehensive information of diseased tissue or organs. At the same time, the redundant information in the source images is abrogated. Hence, the doctor can easily make an accurate diagnosis or determine the accurate therapeutic scheme.

Nowadays, many medical image fusion methods has been proposed such as intensity-hue-saturation (ISH) transform, principal component analysis(PCA), brovey transform[4-5]. In addition, the methods based on multiscale analysis (MCA) methods has been proposed in the latest including the laplacian transform, the discrete wavelet transform

ISSN: 2005-4254 IJSIP

(DWT) [6], the nonsubsampled contourlet transform (NSCT) [7] and shearlet transform [8]. The limitations of wavelet direction make it does not perform well multi-dimensional data such as image. Therefore, DWT-based fusion schemes cannot preserve the salient features of the source images efficiently [9]. Furthermore, the redundancy in shearlet [10] and NSCT [11] decomposition make the runtime very slow in image processing including image fusion, although the shearlet and NSCT can capture the point discontinuities of image and track the curve directions of images. In comparison with wavelet transform, the multiwavelet is orthogonal and symmetric but possesses the property of compact support [12]. However, it is difficult to express the geometry structures of images in consideration of the multiwavelet is isotropy characteristic. The nonsubsampled direction filter bank (NSDFB) [13] has shift-invariant property because the downsampling and upsampling in the direction filter bank (DFB) [14] is eliminated in NSDFB. Hence, the NSDFB is iteratively employed in NSCT to decompose the image into many directions. Inspired by the fact that the laplacian transform is combined with the directional filter bank in Contourlet transform[14], we propose a new image multi-resolution and multi-scale representation method named as Multi-NSDFB transform that the multiwavelet transform is combined with NSDFB in this paper. In Multi-NSDFB transform, the image is decomposed into a low-pass subband and three high-pass subbands by the multiwavelet transform and the NSDFB is subsequently performed to decompose the every subband into several direction coefficients. Therefore, the Multi-NSDFB transform is a multi-resolution, multidirectional, multi-scale and anisotropic expression for effectively capturing the detailed information in multimodal medical images.

2. Multi-NSDFB Transform

2.1. Multiwavelet

Goodman firstly constructed the multiwavelet in 1994 [15]. G. Donovan applies the fractal interpolation approach to reconstruct the Geronimo, Hardin and Massopust (GHM) multiwavelet which support basis is in [0 2] [16]. Multiwavelet is orthogonal, symmetric, high approximation and good regularity. Both the multiwavelet and the scalar wavelet are based on multiscale geometry analysis theory. Multiwavelet is composed of the scale function $\Phi(t) = [\phi_1(t), \phi_2(t), \ldots \phi_r(t)]^T$ and the wavelet function $\Psi(t) = [\psi_1(t), \psi_2(t), \ldots \psi_r(t)]^T$ after translation and expansion [17-19]. The multiwavelet two-scale equations verified the following:

$$\Phi(t) = \sqrt{2}\sum_{k=0}^{L} H_k \Phi(2t-k) \quad k \in Z \tag{1}$$

$$\Psi(t) = \sqrt{2}\sum_{k=0}^{L} G_k \Psi(2t-k) \quad k \in Z \tag{2}$$

Where l is the number of scaling coefficients and H_k and G_k are the lowpass and highpass matrix filter for each translation distance k, respectively. There are r ($r = 2$) scaling function in the multiwavelet transform. Similar to traditional wavelet, the decomposition and reconstruction of multiwavelet is as follows:

$$s_{j-1,n} = \sum_k H_{k-2n} s_{j,k} \quad d_{j-1,n} = \sum_k G_{k-2n} s_{j,k} \tag{3}$$

$$s_{j,n} = \sum_k H^*_{k-2n} s_{j-1,k} + \sum_k G^*_{k-2n} d_{j-1,n} \tag{4}$$

Where $s_{j-1,n}$ is the r dimension low frequency component. $d_{j-1,n}$ stands for r dimension high frequency component. $*$ is the conjugate and transpose operation.

2.2. NSDFB

NSDFB is a new kind filter banks used in the nonsubsampled contourlet transform. There are two modules of the two-channel quincunx filter banks and the shearing operation in the NSDFB. The 2-D images can be divided into the horizontal directions and the vertical direction by the two-channel quincunx filter banks. The second module is executed before the end of the decomposition of quincunx filtering, and after the composite phase, it conducts an anti-shearing operation. Its function is reordering the image sampling. Actually, the shearing operation is a kind of image sampling. After this operation, the image is revolved and the width becomes twice wider then before. The key of NSDFB is that combines the shearing operation with the quincunx filter banks in the points of tree-structure. To achieve multi-direction decomposition, the NSDFB is iteratively used. Figure 1 illustrates a four-channel directional decomposition.

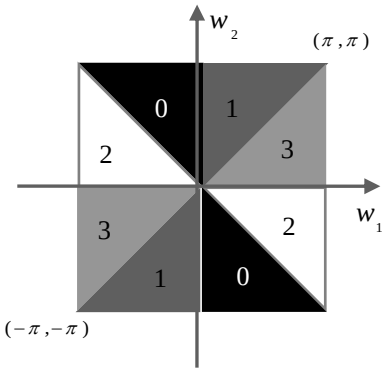

Figure 1. Frequency Partitioning of Four-Channel Direction NSDFB

2.3. The Multi-NSDFB Transform

Other than the NSCT [6], the multiwavelet is combined with the NSDFB named as Multi-NSDFB transform is present. An image is firstly decomposed into a low-pass subband and three high-pass subbands by the multiwavelet transform. Because multiwavelet is orthogonal and symmetric and possesses the property of compact support, every subband above is subsequently decomposed into several directional subbands by the NSDFB. In this paper, the two levels decomposition of the multiwavelet is used. After that, every subbands of multiwavelet is decomposed to four directions by the NSDFB. The decomposition process can clearly be described in the Figure 2.

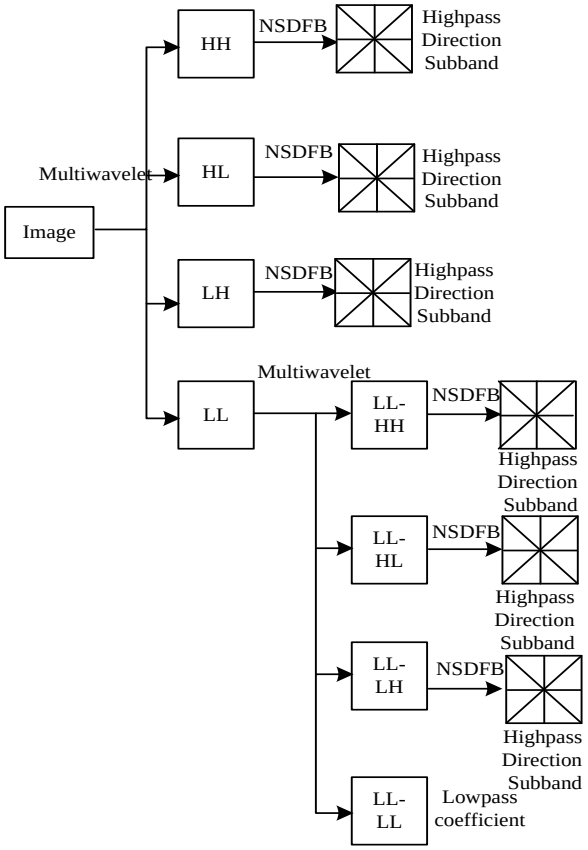

Figure 2. Multi-NSDFB Decomposition of the Image

3. Fusion Rule

3.1. Modified Spatial Frequency

Spatial frequency (SF) [20] is calculated according to the row and column frequency of the image. The image fusion method based on the SF has been proposed by Qu [21]. In this paper, the method of the SF motivated the PCNN is effective to fuse the multifocus image. However, this method is not effective to fuse the multimodal medical images. The SF of the image is not enough to express the salience character because of lacks of the direction information present in the image. The modified spatial frequency is capable of capturing the fine details present in the image because of incorporate the direction information and the row and column frequency. The spatial frequency can be calculated according to the Eq. (5).

$$SF = \frac{1}{MN}\sum_{m=1}^{M}\sum_{n=2}^{N}\left(I_{m,n} - I_{m,n-1}\right)^2 + \left(I_{m,n} - I_{m-1}\right)^2 \tag{5}$$

Where $I_{m,n}$ is the pixel value of the image in the m column and n row in the image I of M column and N row. In this paper, the modified spatial frequency is adopted to evaluate the salience feature in the Multi-NSDFB coefficient. The modified spatial frequency (MSF) consists of traditional spatial frequency (SF) and diagonal frequency (DF). The DF can be expressed as following:

$$DF = \sqrt{\frac{1}{MN}\sum_{m=1}^{M}\sum_{n=1}^{N}\left(I_{m,n} - I_{m-,n-1}\right)^2 + \left(I_{m-1,n} - I_{m,n-1}\right)^2} \tag{6}$$

Then, the modified spatial frequency can be calculated as:

$$MSF = \sqrt{SF_{m,n}^{2} + DF_{m,n}^{2}} \tag{7}$$

3.2. PCNN

Different from the artificially traditional neural network, the pulse coupled neural network (PCNN) conforms to the character of the animals of the brain's visual cortex sync pulse distribution [22]. It is a simplification and approximation of the real neurons, and can be used to various fields of image processing such as image segment, image fusion and image classification. The PCNN is used as a single two-dimensional network of local connection network in the filed of image processing. The number of neuron is equal to pixel's value of the input image [23]. Then, each neuron is connected with its correspondent pixel and the adjacent neuron at the same time. The model of PCNN neuron can be described as the following:

$$F_{ij}[n] = \exp(-\alpha_F)F_{ij}[n-1] + V_F \sum m_{ij}^{kl} Y_{kl}[n-1] + I_{ij} \tag{8}$$

$$L_{ij}[n] = \exp(-\alpha_L)L_{ij}[n-1] + V_L \sum w_{ij}^{kl} Y_{kl}[n-1] \tag{9}$$

$$U_{ij}[n] = F_{ij}[n](1 + \beta L_{ij}[n]) \tag{10}$$

$$Y_{ij}[n] = 1, \quad if \quad U_{ij}[n] > E_{ij}[n] \tag{11}$$

$$Y_{ij}[n] = 0, \quad otherwise \tag{12}$$

$$E_{ij}[n] = \exp(-\alpha_E)E_{ij}[n-1] + V_E \sum Y_{kl}[n-1]F \tag{13}$$

In PCNN model, the neuron receives input signals from feeding and linking inputs through the receptive field. Then, input signals are divided into two channels. One channel is feeding input F_{ij} and the other is linking input. L_{ij} I_{ij} is the input stimulus such as the normalized gray level of image pixels in (i, j) position. U_{ij} is the internal activity of neuron, and E_{ij} is the dynamic threshold. Y_{ij} stands for the pulse output of neuron and it gets either the binary value 0 or 1. The interconnections *m* and *w* are the synaptic gain strengths for the feeding and the linking inputs, respectively, which is dependent on the distance between neurons. α_L , α_F and α_E are the attenuation time constants of L_{ij} , F_{ij} and E_{ij} , respectively. β is the linking strength. V_F ,V_E are normalizing constants. Where, *n* denotes the current iteration (discrete time step) and varies from 1 to Nmax (the total number of iterations).

4. Proposed Method

1. The proposed Multi-NSDFB transform are used to decompose the source medical images, respectively.

2. Compute the $MSF_B^{l,k}(u,v)$ and $MSF_A^{l,k}(u,v)$ of the all every subband according to Eq. (7), separately.

3. Adopt the $MSF_B^{l,k}(u,v)$ and $MSF_A^{l,k}(u,v)$ to motivate the PCNN, respectively. Firing times $T_{A,uv}^{l,k}(n)$ and $T_{B,uv}^{l,k}(n)$ should be calculated by:

$$T_{u,v}^{l,k}(n) = T_{u,v}^{l,k}(n-1) + Y_{u,v}^{l,k}(n) \tag{14}$$

When the iteration process stopped. The decision map $D_{uv}^{l,k}$ by (10). The coefficients can be fused by (16).

$$D_{F,u,v}^{l,k} = \begin{cases} 1 & if \quad T_{A,u,v}^{l,k}(n) \geq T_{B,u,v}^{l,k}(n) \\ 0 & if \quad T_{A,u,v}^{l,k}(n) \leq T_{B,u,v}^{l,k}(n) \end{cases} \tag{15}$$

$$Multi_{F,uv}^{l,k} = \begin{cases} Multi_{A,uv}^{l,k} & if \quad D_{u,v}^{l,k} = 1 \\ Multi_{B,uv}^{l,k} & if \quad D_{u,v}^{l,k} = 0 \end{cases} \tag{16}$$

The $Multi_{F,uv}^{l,k}$, $Multi_{A,uv}^{l,k}$ and $Multi_{B,uv}^{l,k}$ are the coefficient of the fused images F, source image A and source image B located at the *u*-th row and *v*-th column in the *l*-th scale and *k*-th direction subband, respectively.

4. Finally, the inverse Multi-NSDFB transform are adopted to reconstruct the fused medical images by $Multi_{F,uv}^{l,k}$.

5. Experimental Results and Analysis

To evaluate the performance of the proposed fusion rule, five experiments have been performed as shown in Figure 3, respectively. These images are characterized in three different groups: 1) CT-MRI, 2) MR-T1-MR-T2 and 3) MR-GAD-MRI-T1 images. The group d in Figure 3 are MRI-T1 and T1-weighted MR-GAD images whereas the group a, b and c in Figure 3 are T1-weighted MR image (MR-T1) and T2-weighted MR image (MR-T2), respectively. The group e in Figure 3 is the CT and MRI images, respectively. The corresponding pixels of two input images have been perfectly matched. All images have the same size of 256×256 pixel, with 256-level gray scale.

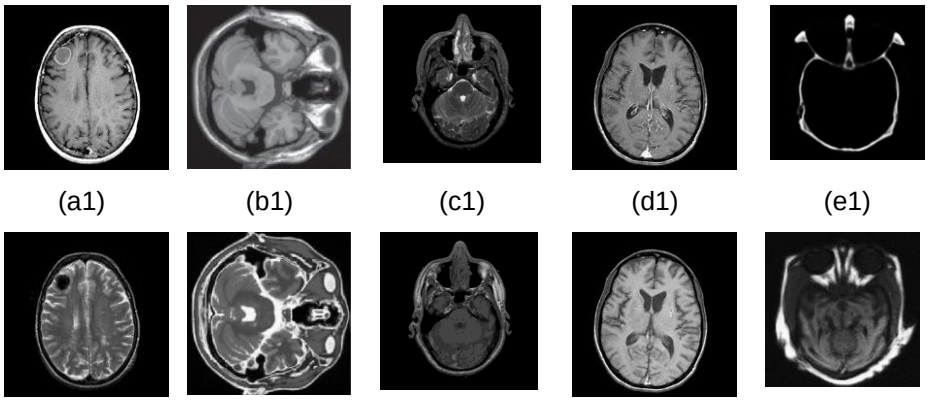

Figure 3. Several Kinds of Multimadal Medical Images

For comparison purposes, in this paper, the fusion is performed using the redundant discrete wavelet transform (RDWT) method [24], the Ripplet method [25] and proposed Multi-NSDFB transform method. In the RDWT method, the source images are decomposed by two levels and 'db6' wavelet filters. The low frequency coefficients are fuse by the max fusion rule. The entropy of each block size 3×3 is used to fuse the three detailed subbands. In the Ripplet method, The parameters of the '9/7' filter, 'pkva' filter

and levels= [0-3] are used to decompose the source images by Ripplet transom. Parameters of PCNN are set as 3×3, α_L = 0.06931, α_θ = 0.2, β = 0.2, V_L = 1.0, V_θ = 20. The maximal iterative number is 200. M = $[\sqrt{2},1,\sqrt{2};0,1,0;\sqrt{2},1,\sqrt{2}]$.

The fusion medical image of MRI-T1 and MRI-T2 with the different method is demonstrated in the Figure 4 and Figure 5. From the fusion results of the two methods in Figure 5 (a-c), it is easy to find that with all the methods the fused image now contains both the MRI-T1 information and MRI-T2 information. However, some difference can be clearly seen by careful observation in Figure 5. It can be clearly seen that the Figure 4 (c), Figure 4 (f) and Figure 4 (i) fused by proposed method is more clear than the other images fused by the other two methods. Samely, the Figure 5(c) is clearer than the Figure 5(a) and Figure 5(b). Furthermore, the fused medical image of CT and MRI with the proposed method is done. From the fusion results of the three methods in Figure 6 (a)-(c), it is easy to find that with all the methods the fused image now contains both the bones information and tissues information, which cannot be seen in the separate CT or MRI image. However, some different can be clearly seen by careful observation in Figure 6. It can be clearly seen that there is a highest contrast in the image fused by proposed method than in those by the other three methods.

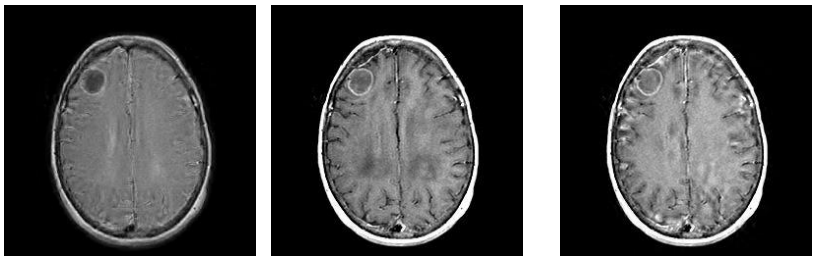

(a) RDWT (b) Ripplet (c) Proposed Method

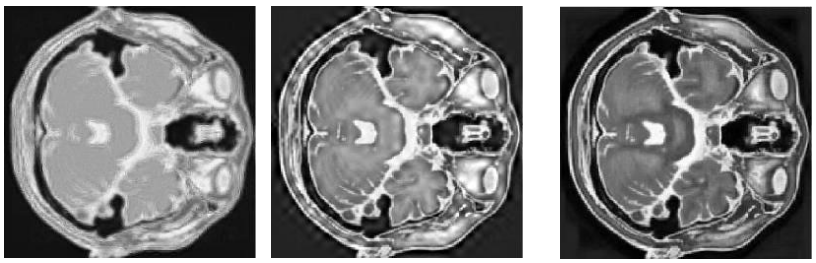

(d) RDWT (e) Ripplet (f) Proposed Method

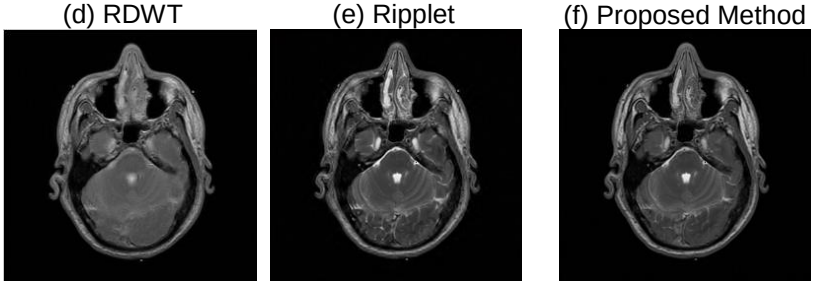

(g) RDWT (h) Ripplet (i) Proposed Method

Figure 4. The Fusion Results of MRI-T1-MRI-T2

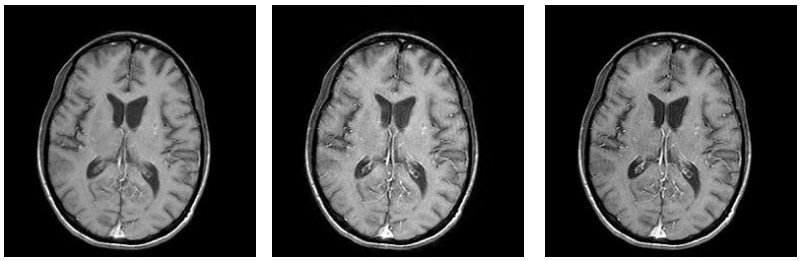

(a) RDWT (b) Ripplet (c) Proposed Method

Figure 5. The fusion results of MRI-T1-MRI-GAD

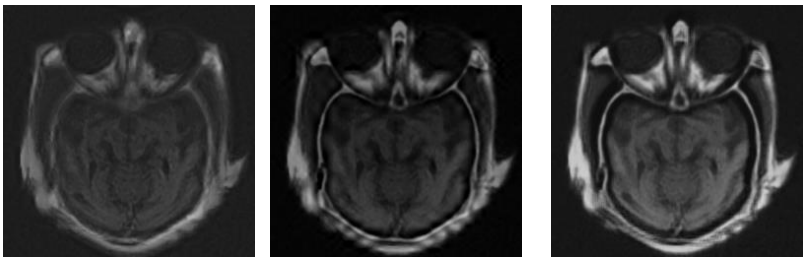

(a) RDWT (b) Ripplet (c) Proposed Method

Figure 6. The Fusion Results of CT-MRI

For further comparison beside the subjective visual observation above, two objective criteria of the MI [27] and $QAB^{/F}$ [28] values are adopted to compare the fusion result of the four approaches. The MI and $Q^{AB/F}$ values of the fused multimodal medical images are listed in Table 1. We observe that using different fusion methods leads to different objective criteria performances. It can be seen from Table 1 that the MI and $Q^{AB/F}$ value of the proposed algorithm are the largest in the two methods, and the MI and $Q^{AB/F}$ value of the RDWT method is the smallest. From Figure 4 and Figure 5. It is easy to be concluded, just as Table 1, that the results presented in these examples can demonstrate that our method can fuse the source images while retaining much more information than that of the other two methods. The objective evaluation results of MI and $Q^{AB/F}$ coincide with the visual effect analyzed in above three paragraphs very well. From what has been discussed above, it may be concluded that the proposed algorithm can do well in the fusion such as multi modal medical images and perform better than the RDWT and Ripplet-MSF-PCNN approaches, based on in terms of objective performance and subjective performance, provides the best performance in three kinds of images fusion.

Table 1. The Comparison on Objective Metrics

Image	Criteria	**R**DWT	Ripplet	Proposed method
Group a	MI	3.0094	3.4168	**3.5469**
	$Q^{AB/F}$	0.2149	0.2784	**0.5699**
Group b	MI	3.9029	3.8567	**4.4394**
	$Q^{AB/F}$	0.2317	0.5673	**0.6506**
Group c	MI	3.4261	3.802	**3.556**
	$Q^{AB/F}$	0.5059	0.62	**0.6943**
Group d	MI	3.5207	3.8342	**4.0555**
	$Q^{AB/F}$	0.346	0.3652	**0.6988**
Group e	MI	2.4211	2.7964	**4.004**
	$Q^{AB/F}$	0.3679	0.397	**0.7210**

6. Conclusion

In order to improve the effect of multi-modal medical image fusion and increase diagnostic accuracy, a novel medical image fusion algorithm is present in this paper. The multiwavelet is combined with the NSDFB to construct the proposed Multi-NSDFB transform. The proposed Multi-NSDFB transform is not only a 2D image sparse representation method but also a kind of better approximation of image edge. Furthermore, The Multi-NSDFB transform has the characteristic of multi-scale, multi-direction and anisotropy. The experiments of the CT-MRI, MRI-T1-MRI-T2 medical images fusion indicate that the suggested fusion scheme is more effective than other image fusion works such as RDWT and Ripplet.

Acknowledgments

Some of the images adopted in these experiments are downloaded from the website of http: //www.imagefusion.org and http://www.med.harvard.edu/AANLIB/home.html. This research was partially sponsored by the Natural Science Fund of Hebei Province under grant F2013210094 and F2013210109.

References

[1] H. Torsten, B. Julie, N. V. Ruiter, M. Sak and D. Neb, "2D/3D image fusion of x-ray mammograms with speed of sound images: Evaluation and visualization", Progress in Biomedical Optics and Imaging, Proceedings of SPIE, 7968, (**2011)**.
[2] C. T. Kavitha and C. Chellamuthu, "Medical image fusion based on hybrid intelligence", Applied Soft Computing, vol. 20, **(2014)**, pp. 83-94.
[3] A. P. James and B. V. Dasarathy, "Medical image fusion: A survey of the state of the art", Information Fusion, vol. 19, **(2014)**, pp. 4-19.
[4] Q. G. Miao and B. S. Wang, "A novel image fusion algorithm using FRIT AND PCA", Tenth International Conference on Information Fusion, Quebec, **(2007)**.
[5] J. Yonghong, "(1998) Fusion of landsat TM and SAR images based on principal component analysis", Remote sensing technology application, vol. **(2013)**, pp. 46-49.
[6] L. Yang, B. L. Guo and W. Ni, "Multimodality medical image fusion based on multiscale geometric analysis of contourlet transform", Neurocomputing, vol. 72, no. 3, **(2008)**, pp. 203-211.
[7] D. Cunha, L. Arthur, J. Zhou and N. Do Minh, "The nonsubsampled contourlet transform: Theory, design, and applications", IEEE Transactions on Image Processing, **(2006)**, pp. 3089-3101.
[8] G. Deep, A. R. Shyam and T. Barjeev, "Edge preserved enhancement of medical images using adaptive fusion-based denoising by shearlet transform and total variation algorithm", Journal of Electronic Imaging, vol. 22, no. 4, **(2013)**.
[9] Y. Yang, D. S. Park, S. Huang and N. Rao, "Medical Image Fusion via an Effective Wavelet-Based Approach", EURASIP Journal on Advances in Signal Processing, 579341 doi:10.1155/2010/579341 **(2010)**.
[10] L. Wang, B. Li and Lian-fang Tian, "Multi-modal medical image fusion using the inter-scale and intra-scale dependencies between image shift-invariant shearlet coefficients", Information Fusion, vol. 19, **(2014)**, pp. 20-28.
[11] D. Sudeb and K. M. Kumar, "NSCT-based multimodal medical image fusion using pulse-coupled neural network and modified spatial frequency", Medical and Biological Engineering and Computing, vol. 50, no. 10, **(2012)**, pp. 1105-1114.
[12] J. Chen, O. Xun, W. Zheng, J. Xu, J. Zhou and S. Yu. "The application of symmetric orthogonal multiwavelets and prefilter technique for image compression", Multimedia Tools and Applications, vol. 29, **(2006)**, pp.175-187.
[13] M. Liyong and F. Naizhang, "Nonsubsampled contourlet transform based image fusion for ultrasound tomography", Journal of Nanoelectronics and Optoelectronics, vol. 7, no. 2, **(2012)**, pp. 216-219.
[14] N. Do Minh and V. Martin, "The contourlet transform: An efficient directional multiresolution image representation", IEEE Transactions on Image Processing, vol. 12, **(2005)**, pp. 2091-2106.
[15] T. N. T. Goodman and S. L. Lee, "Wavelets of multiplicity, Transactions of the American Mathematical Society", vol. 342, **(1994)**, pp. 307-324.
[16] C. Zhao, X. Zhong, Q. Dang and L. Zhao. "De-noising signal of the quartz flexural accelerometer by multiwavelet shrinkage", International Journal on Smart Sensing and Intelligent Systems, vol. 6, **(2013)**, pp. 191-208.
[17] L. Shen, H. H. Tan and J. Y. Tham, "Symmetric-Antisymmetric Orthonormal Multiwavelets and Related Scalar Wavelets", Applied and Computational Harmonic Analysis, vol. 8, **(2000)**, pp. 258-279.

[18] Z. Lin, Z. J. Fang, S. Wang, Y. Fan and G. D. Liu, "Multiwavelet adaptive denoising method based on genetic algorithm", Journal of Infrared and Millimeter Waves, vol. 28, **(2009)**, pp. 77-80.
[19] H. Wang, "A new Multiwavelet-based approach to image fusion", Journal of Mathematical Imaging and Vision, vol. 21, **(2004)**, pp. 177-192.
[20] A. Eskicioglu, "Fisher P Image quality measures and their performance", IEEE Transactionon Communication, vol. 43, no. 12, **(1995)**, pp. 2959-2965.
[21] Q. XiaoBo, Y. JingWen, X. HongZhi and Z. ZiQian, "Image fusion algorithm based on spatial frequency-motivated pulse coupled neural networks in nonsubsampled" Acta Autom Sin, vol. 34, no. 12, **(2008)**, pp. 1508-1514.
[22] M. M. Subashini and S. K. Sahoo, "Pulse coupled neural networks and its applications", Expert Systems with Applications, vol. 41, no. 8, **(2014)**, pp. 3965-3974.
[23] L. Yunxia, Y. Zhang and L. Jian Cheng, "Support vector set selection using pulse-coupled neural networks", Neural computing and application, vol. 25, no. 2, **(2014)**, pp. 401-410.
[24] S. Richa, V. Mayank and N. Afzel, "Multimodal medical image fusion using Redundant Discrete Wavelet Transform", Proceedings of the 7th International Conference on Advances in Pattern Recognition, **(2009)**, pp. 232-235.
[25] D. Sudeb and K. M. Kumar, "Ripplet based multimodality Medical Image Fusion using Pulse-Coupled Neural Network and Modified Spatial Frequency", 2011 International Conference on Recent Trends in Information Systems, **(2011**), pp. 229-234.
[26] Y. Yang, S. Tong, S. Huang and P. Lin, "Log-Gabor Energy Based Multimodal Medical Image Fusion in NSCT Domain", Computational and Mathematical Methods in Medicine, http://dx.doi.org/10.1155/2014/835481, **(2014)**.
[27] G. Piella, "A general framework for multiresolution image fusion: from pixels to regions", Information Fusion, vol. 4, no. 4, **(2003)**, pp. 259-280.
[28] V. Petrovic and C. Xydeas, "Objective image fusion performance characterization", Proceedings of the International Conference on Computer Vision, vol. 2, **(2005)**, pp. 1866-871.

Author

Peng Geng received his Master in the Department of Information Engineering from Shijiazhuang Tiedao University in 2007, and received his B.S. degree from Hebei Normal University in 2001, respectively. He is currently an Associate Professor in the school of information science and technology, Shijiazhuang Tiedao University. His current research interests are focused on image fusion, multiscale geometry analysis.

